Sodium-Containing Spinel Zinc Ferrite as a Catalyst Precursor for the Selective Synthesis of Liquid Hydrocarbon Fuels

Yo Han Choi,[a] Eun Cheol Ra,[b] Eun Hyup Kim,[b] Kwang Young Kim,[b] Youn Jeong Jang,[a] Kyeong-Nam Kang,[b] Sun Hee Choi,[a] Ji-Hyun Jang,[b] and Jae Sung Lee*[b]

A microwave-assisted hydrothermal synthesis produces $ZnFe_2O_4$ containing Na residue as a precursor to a CO_2 hydrogenation catalyst that displays high CO_2 conversion and high selectivity to liquid hydrocarbon products in the gasoline and diesel range with high olefin-to-paraffin ratios. Compared to reference catalysts derived from Fe_2O_3 and a $ZnO–Fe_2O_3$ physical mixture, the $ZnFe_2O_4$-derived catalyst contains well-dispersed iron particles with Zn serving as a structural promoter. A profound effect of the residual Na as an electronic promoter is also observed, which improves the selectivity for C_{5+} hydrocarbons and olefins. The $ZnFe_2O_4$-derived catalyst exhibits excellent performance in the CO_2 Fischer–Tropsch reaction as it forms the active Hägg iron carbide (χ-Fe_5C_2) phase readily through the in situ carburization of iron.

Introduction

Global warming caused by the greenhouse effect of anthropogenic CO_2 in the atmosphere is a serious issue that threatens the future of humankind.[1] Carbon capture and storage (CCS) has been considered as an effective and aggressive measure to counter the problem.[2] However, the storage of CO_2 in geological or ocean reservoirs has serious drawbacks such as possible leakage, long-term liability, and the availability of sufficient storage capacity in many regions of the world. By contrast, in carbon capture and utilization (CCU), the captured CO_2 is converted into useful products such as fuels, chemicals, plastics, and alternative building materials.[3] Among the many possible CCU products, transportation fuels are the most attractive because of their huge market size, which could accommodate the large amount of CO_2 released from industrial vent streams.[4–6] In particular, liquid hydrocarbon fuels such as gasoline, diesel, and jet fuel are convenient for transportation and storage and readily adaptable to the current distribution infrastructure.

The synthesis of hydrocarbon fuels by CO_2 hydrogenation involves two consecutive reactions, namely, the reverse water–gas shift (RWGS) and Fischer–Tropsch (FT) reactions [Eqs. (1) and (2), respectively].[7]

$$CO_2 + H_2 \rightleftharpoons CO + H_2O \quad \Delta H_{298} = +41\,\text{kJ mol}^{-1} \tag{1}$$

$$CO + 2\,H_2 \rightarrow (CH_2)_n + H_2O \quad \Delta H_{298} = -152\,\text{kJ mol}^{-1} \tag{2}$$

Compared to the conventional CO FT reaction with synthesis gas, CO_2 hydrogenation requires one more H_2 molecule per molecule of CO_2 and produces more of the water byproduct, which is a deactivating agent for FT catalysts. In addition, the thermodynamic barrier of the RWGS reaction limits the CO_2 conversion below 300 °C and 10 bar.[8] Thus, the major challenges in the hydrogenation of CO_2 to liquid fuels are the activation of thermodynamically and kinetically stable CO_2 molecules and the control of the product selectivity toward heavy hydrocarbons instead of undesired methane. Owing to the need for RWGS activity, catalyst selection is confined to Fe instead of other common FT catalysts such as Co, Ni, and Ru.[1]

The hydrogenation of CO_2 over iron-based FT catalysts under typical reaction conditions produces mainly methane. There have been extensive studies to produce more useful heavier hydrocarbon products. For example, an iron catalyst derived from Fe_2O_3 synthesized by a template-assisted method yielded a high CO_2 conversion and a good C_2–C_4 hydrocarbon selectivity in CO_2 hydrogenation at 15 bar and 627 K with a H_2/CO_2 ratio of 3:1.[9] In another recent study, $MnFeO_x$ nanocomposites were active and selective toward C_2–C_4 synthesis.[10] To improve CO_2 conversions and heavy-hydrocarbon selectivity, iron-based catalysts are commonly modified with a metal oxide (α-Al_2O_3 or TiO_2), carbon supports such as N-doped materials, and alkaline promoters.[8,11] In spite of these efforts, selectivity to liquid products heavier than C_5 (C_{5+}) remained below 40%. Recently, our group reported that a Cu–Fe catalyst derived from delafossite $CuFeO_2$ could produce C_{5+} products with selectivity greater than 60%.[12] Since then, the direct conversion of CO_2 to gasoline fuel over Na-Fe_3O_4/HZSM-5 as catalyst was reported.[13] As these catalysts result in the selective formation of heavy hydro-

[a] Y. H. Choi, Dr. Y. J. Jang, Dr. S. H. Choi
Division of Advanced Nuclear Engineering
Pohang Accelerator Laboratory
Pohang University of Science and Technology (POSTECH)
Pohang, 790-784 (Korea)

[b] E. C. Ra, E. H. Kim, K. Y. Kim, K.-N. Kang, Prof. J.-H. Jang, Prof. J. S. Lee
School of Energy and Chemical Engineering
Ulsan National Institute of Science and Technology (UNIST)
Ulsan, 44919 (Korea)
E-mail: jlee1234@unist.ac.kr

Supporting Information and the ORCID identification number(s) for the author(s) of this article can be found under https://doi.org/10.1002/cssc.201701437.

carbons in a similar fashion to the CO FT catalysts, they could be called "CO_2 FT catalysts". The catalysts form Hägg iron carbide (χ-Fe_5C_2) readily through the in situ carburization of Fe during CO_2 hydrogenation, and χ-Fe_5C_2 is the known active phase of iron CO FT catalysts.

In the presented work, we synthesize Na-containing $ZnFe_2O_4$ as a new Fe–Zn catalyst precursor through a simple microwave-assisted hydrothermal method. During the pre-reduction step with H_2, $ZnFe_2O_4$ is reduced to metallic Fe decorated with Zn nanoparticles containing Na residue derived from the synthesis step. The Zn serves as a structural promoter to suppress the growth of Fe particles, whereas the Na serves as an electronic promoter to modify the catalytic activity and selectivity of the Fe particles for CO_2 hydrogenation. The beneficial effect of the Zn and Na promoters results in the facile in situ formation of the χ-Fe_5C_2 phase. As a result, our new Fe–Zn catalyst derived from $ZnFe_2O_4$ (ex-$ZnFe_2O_4$) overcomes the common barriers of CO_2 FT catalysts, and high CO_2 conversions as well as high selectivities to liquid fuels can be achieved.

Results and Discussion

Physicochemical properties of the catalysts

We synthesized $ZnFe_2O_4$ by a microwave-assisted hydrothermal method to obtain small particle sizes and high surface areas, as described in the Experimental Section. As reference catalyst precursors, Fe_2O_3, a ZnO–Fe_2O_3 physical mixture (Zn/Fe molar ratio 1:2), and Na-free $ZnFe_2O_4$ were also synthesized. The powder XRD patterns (Figure 1 a) exhibit intense diffraction peaks at $2\theta = 34$ and 36° for Fe_2O_3 and broad peaks at $2\theta = 30$ and 35° for the spinel $ZnFe_2O_4$ phase. The physically mixed Fe_2O_3–ZnO sample shows the peaks of both ZnO and Fe_2O_3. All catalyst precursors were pre-reduced in a H_2 flow at 400 °C for 2 h immediately before the reactions (Figure S1, Supporting Information). They showed different degrees of reduction to metallic Fe and Zn phases. The ex-$ZnFe_2O_4$ and ZnO–Fe_2O_3-derived (ex-ZnO–Fe_2O_3) catalysts both reveal metallic Fe and FeO at $2\theta = 41.7$ and 44.6°, respectively. The XRD pattern of the reduced Fe_2O_3 sample (ex-Fe_2O_3) indicates the formation of pure iron metal. An interaction between iron and zinc apparently suppresses the complete reduction of the oxide precursors under the reduction conditions.

The textures catalyst were examined by scanning electron microscopy (SEM) and N_2 sorption (Figure S2 and Table S1). The Fe_2O_3 and ZnO–Fe_2O_3 catalysts are composed of small nanoparticles of approximately 200–300 nm (SEM images) with low surface areas (8 and 20.4 $m^2 g^{-1}$, respectively) and small pore volumes (0.17 and 0.19 $cm^3 g^{-1}$, respectively; Figure S3). The SEM image of reduced Fe_2O_3 shows severe agglomeration (Figure S4 a). As a result of the addition of ZnO to Fe_2O_3, the Fe_2O_3 particle size becomes smaller and the agglomeration caused by reduction is not significant (Figures S3 b and S4 b). The $ZnFe_2O_4$ synthesized by a microwave-assisted hydrothermal method has a much higher surface area (119 $m^2 g^{-1}$) and pore volume (0.33 $cm^3 g^{-1}$). Its SEM image (Figure 1 c) shows clusters of small $ZnFe_2O_4$ particles, and the small size is almost maintained after the reduction (Figure 4 c). This microwave-assisted hydrothermal method allows the swift synthesis of small and stable $ZnFe_2O_4$ particles at a much lower temperature of 180 °C compared with those for other methods involving a high-temperature calcination step.[14]

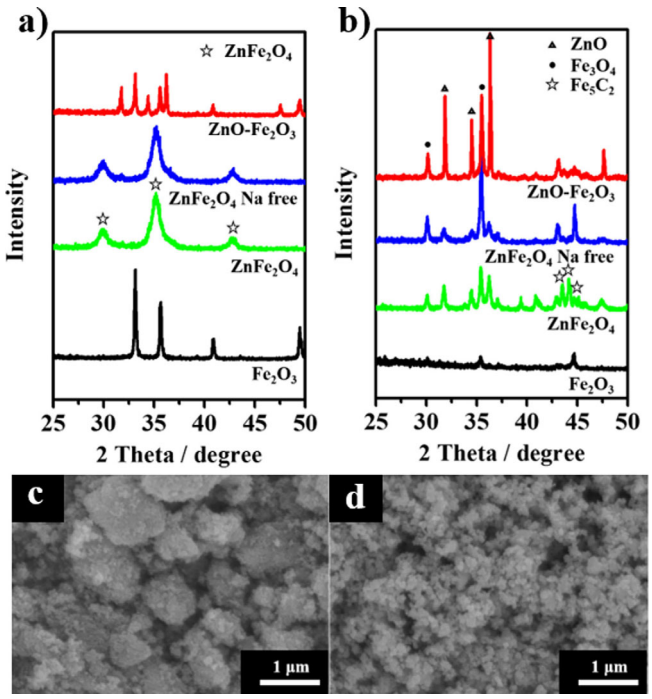

Figure 1. a) Powder XRD patterns of Fe_2O_3, ZnO–Fe_2O_3, $ZnFe_2O_4$, and Na-free $ZnFe_2O_4$. b) XRD patterns of the catalysts after the CO_2 FT reaction for 48 h. SEM images of $ZnFe_2O_4$ c) before and d) after the reaction.

Catalytic CO_2 hydrogenation

The CO_2 hydrogenations over the prepared catalysts were performed in a fixed-bed reactor with a continuous feed of H_2/CO_2 (3:1) and a gas hourly space velocity (GHSV) of 1800 mL $g^{-1} h^{-1}$ at 340 °C and 10 bar. ZnO alone as a reference catalyst caused no CO_2 conversion. As shown in Table 1 and Figure 2, reduced Fe_2O_3 shows a performance typical of iron FT catalysts in CO_2 hydrogenation with a good CO_2 conversion and fair selectivity to C_2–C_4 hydrocarbons. The catalyst derived from the ZnO–Fe_2O_3 mixture exhibits a 36% increase in CO_2 conversion from that for bare Fe_2O_3. The increased CO_2 conversion accompanies increased methane formation at the expense of heavier hydrocarbons. Our new catalyst derived from $ZnFe_2O_4$ synthesized by the microwave-assisted hydrothermal method exhibits a further improved CO_2 conversion (by 86% relative to that of bare Fe_2O_3). In terms of the reaction rates [expressed as Fe time yield (FTY), i.e., moles of CO_2 converted per g of Fe in the catalyst per second], the $ZnFe_2O_4$-derived catalyst shows a significantly higher FTY (3.1 µmol $g_{Fe}^{-1} s^{-1}$) than those of the catalysts derived from bare Fe_2O_3 (1.3 µmol $g_{Fe}^{-1} s^{-1}$) and ZnO–Fe_2O_3 (2.7 µmol $g_{Fe}^{-1} s^{-1}$). However, the most conspicuous characteristic of the $ZnFe_2O_4$-derived catalyst is the selectivity pattern of the hydrocarbon products

Table 1. Steady-state FTY, CO_2 conversion, and product selectivity of various catalysts in CO_2 hydrogenation.[a]

Precursor	FTY[b]	CO_2 conversion [%]	CO selectivity [%]	CO-free HC selectivity [%] C_1	C_2	C_3	C_4	C_{5+}	O/P
Fe_2O_3	1.3	18.2	20.5	40.5	21.4	19.4	10.1	8.6	0.16
$ZnO–Fe_2O_3$	2.7	24.7	23.2	53.1	26.0	13.5	4.5	2.9	0.09
$ZnFe_2O_4$, Na-free	3.0	27.8	21.9	43.6	18.6	17.8	10.5	9.5	0.4
$ZnFe_2O_4$[c]	3.7	34.0	11.7	9.7	8.0	13.0	10.8	58.5	11.3

[a] Reaction conditions: 340 °C, 10 bar, 1800 mL $g^{-1}h^{-1}$, $H_2/CO_2=3$. [b] FTY in $\mu mol_{CO_2}\ g_{Fe}^{-1}\ s^{-1}$. [c] $ZnFe_2O_4$ containing 0.08 wt% of Na.

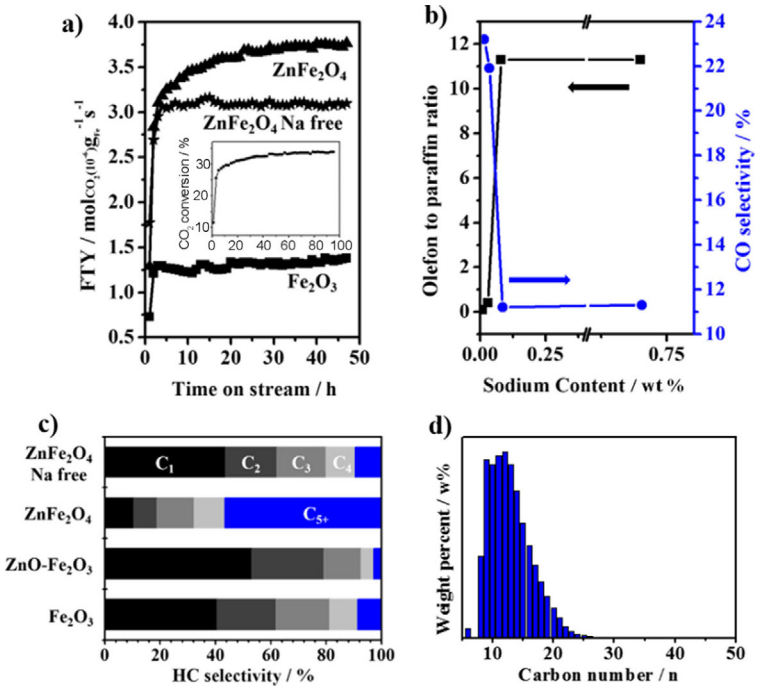

Figure 2. a) FTY versus time on stream for Fe_2O_3, $ZnFe_2O_4$, and Na-free $ZnFe_2O_4$ catalysts. Reaction conditions: 340 °C, 10 bar, 1800 mL $g^{-1}h^{-1}$, $H_2/CO_2=3$. Inset: stability test of $ZnFe_2O_4$ up to 95 h. b) O/P ratios and CO selectivity versus sodium content in $ZnFe_2O_4$. c) CO-free hydrocarbon selectivity of Fe_2O_3, $ZnO–Fe_2O_3$, $ZnFe_2O_4$, and Na-free $ZnFe_2O_4$ catalysts. d) Carbon-number distribution of the liquid products of CO_2 hydrogenation with the $ZnFe_2O_4$-derived catalyst, as determined by a simulated distillation method (ASTM D2887).

from CO_2 hydrogenation. Methane formation is suppressed greatly (40.5→9.7%), and the formation of C_{5+} liquid products increases dramatically (8.6→58%). The collected liquid products were analyzed by a GC simulated distillation method (ASTM D2887) and a detailed hydrocarbon analysis method (ASTM D6729). The products were mostly in the gasoline and diesel range of hydrocarbons (Figure 2d). The product distribution is almost the same as that for typical CO Fischer–Tropsch synthesis over iron-based catalysts.[15] The detailed analysis of the hydrocarbon distribution of the liquid (C_5–C_{11}) products shows that aromatic components represent the largest fraction (≈40.5 wt%), and the olefin fraction is also high (≈26.2 wt%, Figure S5). The performance of the $ZnFe_2O_4$-derived catalyst remained stable in terms of both CO_2 conversion and selectivity over a 95 h stability test (Figure 2a, inset).

Another unique characteristic of our ex-$ZnFe_2O_4$ catalyst in CO_2 hydrogenation is the high olefin/paraffin ratio (O/P) of the C_2–C_4 products of 11.3, which is 70 times higher than that of the ex-Fe_2O_3 catalyst (0.16). For FT synthesis over iron-based catalysts, the alkaline content of the catalyst is generally the most important parameter for the determination of the O/P ratio.[16] The hydrothermal reaction solution for the preparation of the $ZnFe_2O_4$ catalyst contained NaOH to produce basic conditions, and the prepared catalyst contains Na residue. To study the effect of Na, the residual Na content was varied systematically through the variation of the amount of washing after the hydrothermal step. Thus, inductively coupled plasma optical emission spectroscopy (ICP-OES) analysis of the prepared catalyst indicate that the Na content decreased from 0.7 wt% (mild washing with 500 mL of water) to an undetectable level (0%, thorough washing with 6 L of water). As demonstrated in Figure 2b, considerable changes to the O/P ratio and CO selectivity occurred at 0.08 wt% Na. The results are consistent with the well-established roles of Na as (i) an electronic promoter for Fe FT catalysts to shift product distributions to heavier hydrocarbons, (ii) a promotor of CO_2 adsorption through the provision of basic sites,[17] and (iii) an inhibitor of surface hydrogenation.[16,18,19] The Na-free (Na < 0.03 wt%) $ZnFe_2O_4$-derived catalyst shows a decreased CO_2 conversion, a lower C_{5+} selectivity, and a smaller O/P ratio than the Na-containing ex-$ZnFe_2O_4$ (Table 1 and Figure 2c). The CO selectivity also increases if the Na is removed. The RWGS reaction poses a thermodynamic barrier for CO_2 hydrogenation. Alkaline promoters such as Na can donate electrons to Fe metal to promote CO adsorption[20] and accelerate the subsequent CO conversion to hydrocarbons.

The ex-$ZnFe_2O_4$ catalyst was tested for CO hydrogenation ($H_2/CO=3$, 340 °C, 10 bar) to determine its performance under typical CO FT conditions. As shown in Table S2, the ex-$ZnFe_2O_4$ catalyst shows 100% CO conversion (FTY > 11.1 $\mu mol_{CO_2}\ g_{Fe}^{-1}\ s^{-1}$), 45.7% of C_{5+} selectivity, and a high O/P ratio (7.6). The slightly lower C_{5+} selectivity and O/P ratio relative to those for CO_2 hydrogenation seem to originate from the almost complete CO_2 conversion.

Thus, our ex-$ZnFe_2O_4$ catalyst is much more active in CO hydrogenation but similarly selective for C_{5+} hydrocarbons and

olefins. The lower rates of CO_2 hydrogenation are attributed to the reversible RWGS reaction and the competitive adsorption of water.

Role of Na-containing $ZnFe_2O_4$ as efficient CO_2 hydrogenation catalyst precursor

To understand the unique performance of the Na-containing $ZnFe_2O_4$-derived catalyst in the reaction of CO_2 and H_2, the reduction processes of the catalyst precursors were studied through temperature-programmed reduction with H_2 (H_2-TPR). For bare Fe_2O_3, the reduction starts at 270 °C (Figure 3). This

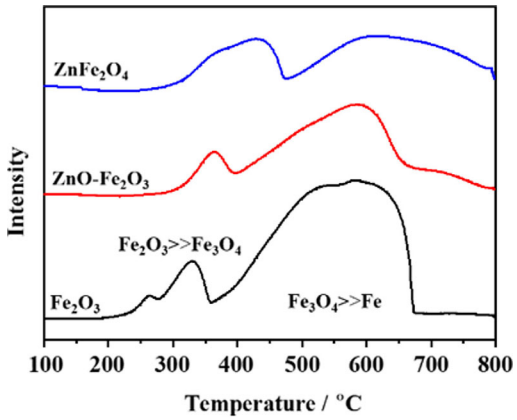

Figure 3. H_2-TPR of Fe_2O_3, ZnO–Fe_2O_3, and $ZnFe_2O_4$.

temperature is substantially lower than that for Fe_2O_3 synthesized by a precipitation method (≈330 °C), probably because of the smaller particle size and the omission of the calcination step. If Fe_2O_3 is combined with ZnO, the reduction temperature increases from 330 to 360 °C. Compared with those for bare Fe_2O_3, the reduction-peak intensities of ZnO–Fe_2O_3 decrease and the peaks are shifted to higher temperatures above 700 °C, because ZnO retards the reduction of Fe_2O_3. The reduction of iron in ZnO–Fe_2O_3 and Fe_2O_3 produces Fe_3O_4 at low temperatures and then metallic Fe at high temperatures. The reduction of $ZnFe_2O_4$ begins at a lower temperature than those for the two reference samples and occurs over a wider temperature range up to 800 °C. These results indicate that a strong interaction between Fe and ZnO retards the reduction of Fe_2O_3. This behavior is also consistent with the XRD pattern in Figure S1, which shows that both ZnO–Fe_2O_3 and $ZnFe_2O_4$ contain the FeO phase after H_2 treatment at 400 °C. Thus, the reduction behavior of the catalysts does not have a significant effect on the catalytic performance.

Next, we performed postreaction analyses of the catalysts after reactions at 340 °C and 10 bar for 48 h. After the reaction, the ex-Fe_2O_3 catalyst shows severe particle aggregation (as shown by the SEM and TEM images in Figures S3 c and S6), which results in a low-surface-area catalyst. The ex-ZnO–Fe_2O_3 catalyst does not show significant morphological changes, and separate rod-type ZnO particles and spherical Fe_3O_4 particles can be observed (Figures S3 d and S7). However, the ex-$ZnFe_2O_4$ catalyst exhibits a dramatically changed morphology; the $ZnFe_2O_4$ precursor decomposes and is reduced into ZnO and metallic Fe particles after the reduction steps (Figures 1 c, d and S4). After the CO_2 hydrogenation reaction, the high-resolution transmission electron microscopy (HRTEM) and electron energy loss spectroscopy (EELS) mapping images (Figure 4) show that small ZnO particles decorate the surfaces of spherical Fe or Fe_3O_4 particles (< 120 nm). The images demonstrate how ZnO works as a structural promoter of Fe; it decorates the surface of Fe or Fe_3O_4 particles to suppress the crystal growth of the Fe particles. If the ZnO and Fe are derived from $ZnFe_2O_4$, the structural promotion effect is more effective than that for the ZnO–Fe_2O_3 physical mixture because of the atomic mixing of Zn and Fe in the $ZnFe_2O_4$ precursor. The XRD pattern in Figure 1 b shows that the main phases of the ex-Fe_2O_3 and ex-ZnO–Fe_2O_3 catalysts are Fe_3O_4 and metallic Fe. Fe_3O_4 is an active phase of the RWGS reaction[21] and must be formed through the partial oxidation of Fe metal by the byproduct water. In contrast, the $ZnFe_2O_4$ catalyst forms the χ-Fe_5C_2 phase through the in situ carburization of iron during the CO_2 hydrogenation, and χ-Fe_5C_2 is the active phase of iron FT catalysts for hydrocarbon synthesis. However, Na-free $ZnFe_2O_4$ shows only Fe_3O_4 and metallic iron phases without the carbide phase after the reaction, and this result highlights the critical role of the small amount of Na residue (≈0.08 wt% in this case) as an electronic promoter.

The postreaction X-ray photoelectron spectroscopy (XPS) analysis (Figure 5) shows that all samples reveal Fe $2p_{3/2}$ and Fe $2p_{1/2}$ peaks at binding energies (BEs) of 711.0 and 723.5 eV, indicating that oxidized Fe species form on the surface because of the water byproduct.[22] This observation matches well with the XRD patterns in Figure 1 b. However, the $ZnFe_2O_4$-derived catalysts show an additional well-defined peak at BE = 707 eV, which could be assigned to iron carbide.[23] The Na-free $ZnFe_2O_4$ also shows the carbide XPS peak but only as a small shoulder peak, which indicates that a much smaller quantity is present than that in the regular $ZnFe_2O_4$ catalyst containing Na.

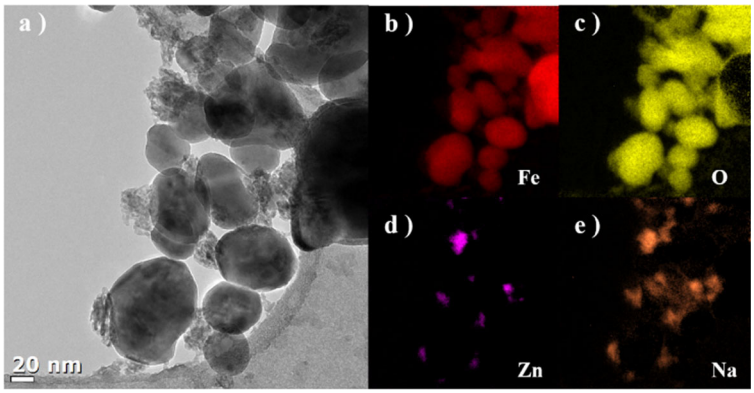

Figure 4. a) HRTEM images of the $ZnFe_2O_4$ catalyst after CO_2 hydrogenation for 48 h. b) Fe, C) O, d) Zn, and e) Na EELS mapping images.

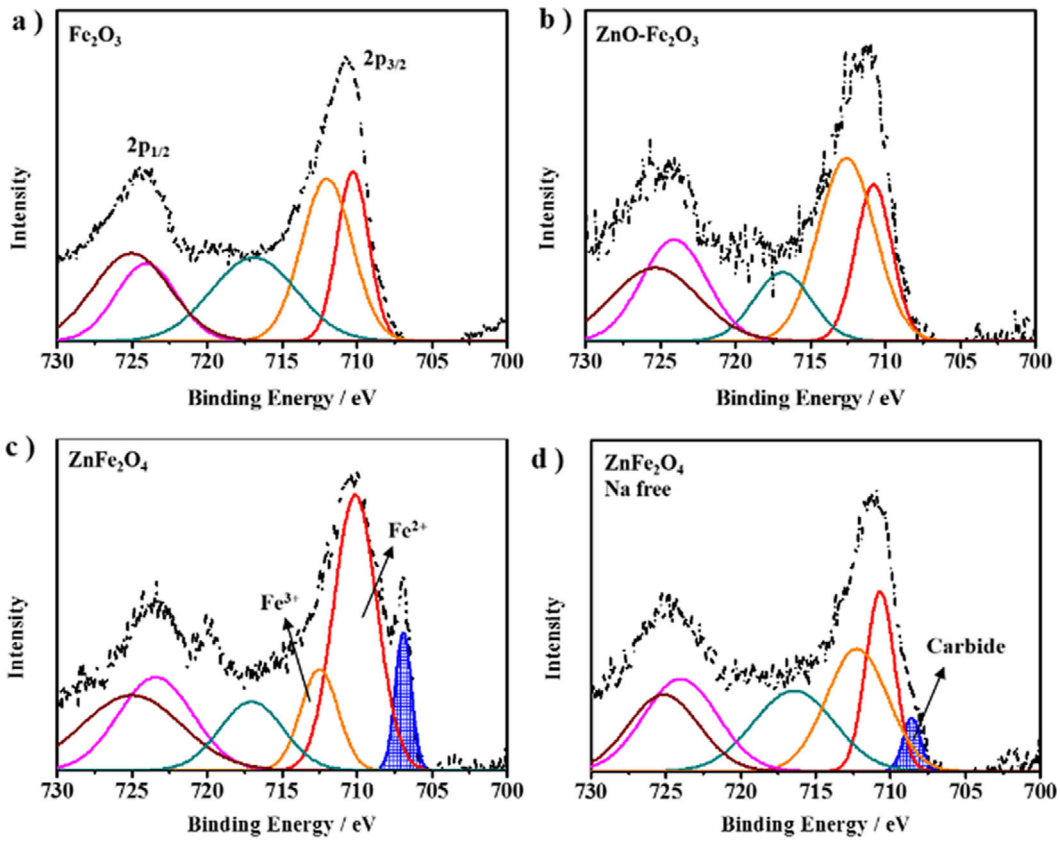

Figure 5. Fe 2p XPS spectra for a) ex-Fe_2O_3, b) ex-ZnO–Fe_2O_3, c) ex-$ZnFe_2O_4$ (Na 0.08 wt%), and d) Na-free ex-$ZnFe_2O_4$ after 48 h of reaction. The iron carbide peaks are highlighted in (c) and (d).

X-ray absorption near-edge structure (XANES) spectroscopy was applied to Fe_2O_3, ZnO–Fe_2O_3, $ZnFe_2O_4$, and Na-free $ZnFe_2O_4$ used for 48 h of CO_2 hydrogenation. The Fe K-edge XANES spectra of the used catalysts as well as that of the reference Fe_5C_2 prepared by a previously reported method are shown in Figure 6a.[24,25] All samples show different shapes for the edge-rising portion in the energy range from 7114 to 7130 eV owing to their different electronic structures. In particular, $ZnFe_2O_4$ and Na-free $ZnFe_2O_4$ present significantly different spectra, which indicate their different chemical states. Only the spectrum of regular (Na-containing) $ZnFe_2O_4$ has a similar pre-edge shape and position to those of the Fe_5C_2 reference at energies of 7114 and 7117 eV. To show the characteristics of the XANES spectra more clearly, the derivative spectra of normalized absorbance are provided in Figure 6b. Again, only ex-$ZnFe_2O_4$ has a spectrum similar to that of the Fe_5C_2 reference.

As mentioned above, ZnO is a structural promoter that retards the sintering of the Fe particle size and, thus, increases the exposure of the active Fe metal surface. Usually, ZnO has a strong interaction with iron particles under FT or CO hydroge-

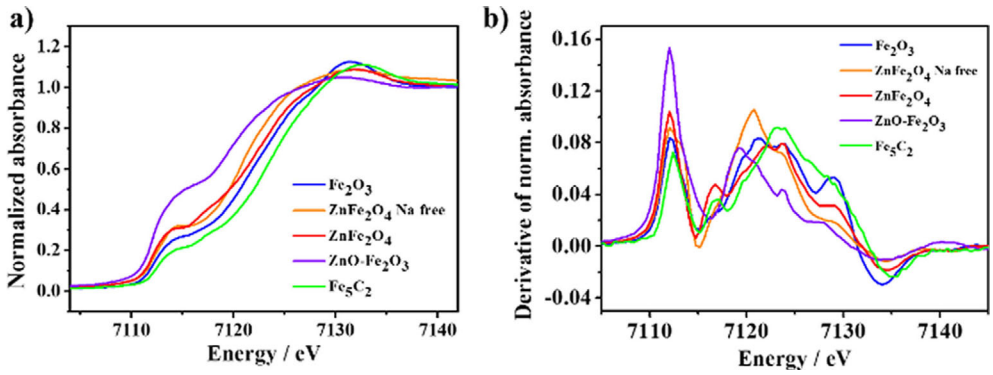

Figure 6. a) Fe K-edge XANES profiles of Fe_2O_3, ZnO–Fe_2O_3, $ZnFe_2O_4$, and Na-free $ZnFe_2O_4$ with the reference Hägg iron carbide. b) Fe K-edge XANES derivative spectra.

nation conditions.[26] In contrast, Na is an electronic promoter that provides electrons to form reduced iron species as the active catalytic sites. Iron metal and Fe_3O_4 are active sites for the formation of hydrocarbons and RWGS reactions, respectively, in FT synthesis.[21,27] Both ZnO–Fe_2O_3 and Na-free $ZnFe_2O_4$ contain Fe and Fe_3O_4 in addition to ZnO (as shown by XRD), which results in the formation of the undesired products methane and short-chain light hydrocarbons. However, $ZnFe_2O_4$ promoted with residual Na as well as Zn can form χ-Fe_5C_2 readily through the in situ carburization of iron during CO_2 hydrogenation. This Hägg iron carbide is the known active phase of iron-based FT catalysts for CO hydrogenation. Our results demonstrate that this phase is also the active phase in CO_2 hydrogenation for the formation of C_{5+} liquid hydrocarbons. Thus, the catalyst presents interesting selectivity for C_{5+} liquid products, high O/P ratios, and high hydrocarbon yields in CO_2 hydrogenation at 340 °C and 10 bar. The evolution of the catalyst structure and the mechanistic idea of a doubly promoted χ-Fe_5C_2 catalyst with electronic (Na) and structural (ZnO) promoters are illustrated in Scheme 1.

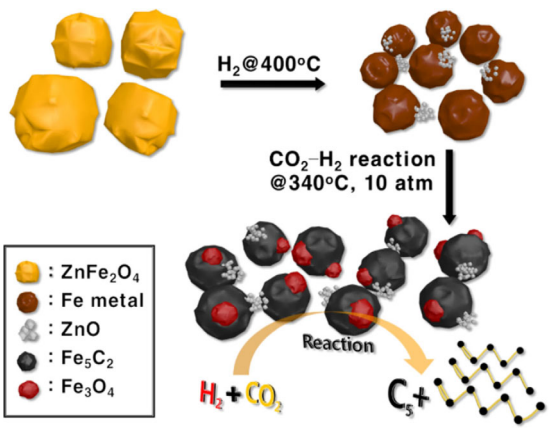

Scheme 1. Structural evolution and mechanistic idea of $ZnFe_2O_4$-derived catalyst for the selective synthesis of C_{5+} liquid fuels by CO_2 hydrogenation.

Conclusions

Sodium-containing $ZnFe_2O_4$ synthesized by a microwave-assisted hydrothermal method becomes an effective catalyst precursor that gives rise to a high CO_2 conversion, an improved liquid-fuel selectivity (≈58%), and a high olefin-to-paraffin ratio (≈11) in CO_2 hydrogenation with the assistance of Zn as a structural promoter and Na as an electronic promoter. The combination of Zn and Na with Fe increases the CO_2 adsorption properties and promotes the in situ formation of Hägg iron carbide, which is the active phase for the formation of heavy hydrocarbons in CO_2 hydrogenation.

Experimental Section

Catalyst preparation

$ZnFe_2O_4$ was synthesized by a microwave-assisted hydrothermal method. $Fe(NO_3)_3 \cdot 9H_2O$ (Kanto, 2.02 g) and $Zn(NO_3)_2 \cdot 6H_2O$ (Zn/Fe = 1:1 molar ratio, 1.47 g) were dissolved in distilled water (40 mL), and NaOH (0.1 mol) was added to the mixture to ensure that it was basic. An excess of the Zn source over the stoichiometry (1:2) was needed to prepare the pure-phase $ZnFe_2O_4$. After a few minutes, propionaldehyde (0.5 mL) was added. The solution was transferred to a 100 mL Teflon tube, which was then placed in a microwave oven (CEM MARS-5, 300 W) for 2 h at 180 °C for the synthesis reaction. After the sample cooled to ambient temperature, it was washed with distilled water (0.5–1.5 L) to control the amount of residual Na. If the samples were washed with more than 6 L of water, the amount of Na residue was negligible, and Na-free $ZnFe_2O_4$ samples were obtained. The Fe_2O_3 reference was also synthesized by a similar microwave-assisted hydrothermal method with only $Fe(NO_3)_3 \cdot 9H_2O$. For the ZnO–Fe_2O_3 physical mixture, commercial ZnO (Sigma–Aldrich) and Fe_2O_3 (Kanto) were mixed in a mortar with a Zn/Fe molar ratio of 1:2.

Catalytic CO_2 hydrogenation

The CO_2 hydrogenation was performed in a fixed-bed reactor at a CO_2/H_2 ratio of 1:3. All samples were pre-reduced in a pure H_2 flow [100 mL min^{-1}, standard temperature and pressure (STP)] at 400 °C for 2 h. After the reduction step, the reactor was purged with Ar to remove the H_2, and then CO_2, H_2, and N_2 (7.69 vol% as an internal reference for GC analysis) entered the reactor at 10 bar and 340 °C with a gas hourly space velocity (GHSV) of 1800 mL g^{-1} h^{-1}. The CO_2, H_2, and N_2 products were analyzed by online GC (Agilent 7890A) with a thermal conductivity detector (TCD, Carboxen 1000 packed column). Hydrocarbons from C_1 to C_6 were analyzed continuously using the same GC instrument with a flame ionization detector (FID, alumina sulfate PLOT capillary column). The heavy-hydrocarbon liquid products were collected in a cold trap. The products were analyzed through simulated distillation (SIMDIS) and detailed hydrocarbon analysis (DHA) based on their carbon-number distributions (ASTM D2887 and D6729).[28]

Characterization and analysis

Powder XRD was performed with a PANalytical X'pert diffractometer with CuK_α radiation (40 mA, 30 kV). H_2-TPR was performed with a Micromeritics AutoChem II apparatus (model 2920). HRTEM and SEM were performed with JEOL JEM-2200FS and Philips Electron Optics XL30S FEG instruments, respectively. The BET surface areas and pore-size distributions were determined from the N_2 sorption isotherms measured at liquid N_2 temperature (Mirae SI, Nanoporosity-XQ). The X-ray absorption fine structure (XAFS) measurements were performed at the 7D beamline of the Pohang Accelerator Laboratory (PLS-II, 3.0 GeV, 400 mA). The synchrotron radiation was monochromatized with Si(111) double crystal monochromators. Under ambient conditions, the Fe K-edge (E_0 = 7112 eV) spectra were collected in transmission mode with He- and N_2-filled IC SPEC ionization chambers. The incident beam was detuned by 30% for the Fe K-edge to reduce contamination by higher harmonics. The spectrum of the Fe foil reference was recorded to enable the calibration of the energy in the spectrum of the sample to the K-edge energy of Fe metal. The AHENA program in the IFEFFIT suite of programs was used to analyze the obtained data to determine the

local structures of the Fe atoms in $ZnFe_2O_4$, Fe_2O_3, and ZnO–Fe_2O_3.[29]

Acknowledgements

This work was supported by the Climate Change Response project (2015M1A2A2074663, 2015M1A2A2056824), the Basic Science Grant (NRF-2015R1A2A1A10054346), Korea Center for Artificial Photosynthesis (KCAP, No. 2009-0093880) funded by MSIP, and MOTIE of Republic of Korea (Project Nos. 10050509 and KIAT N0001754).

Conflict of interest

The authors declare no conflict of interest.

Keywords: carbon dioxide · fischer–tropsch synthesis · fuels · hydrogenation · spinel phases

[1] R. W. Dorner, D. R. Hardy, F. W. Williams, H. D. Willauer, *Energy Environ. Sci.* **2010**, *3*, 884 – 890.
[2] J. Patricio, A. Angelis-Dimakis, A. Castillo-Castillo, Y. Kalmykova, L. Rosado, *J. CO_2 Util.* **2017**, *17*, 50 – 59.
[3] Y. J. Jang, I. Jeong, J. Lee, J. Lee, M. J. Ko, J. S. Lee, *ACS Nano* **2016**, *10*, 6980 – 6987.
[4] J. Wang, S.-M. Lu, J. Li, C. Li, *Chem. Commun.* **2015**, *51*, 17615 – 17618.
[5] T. Witoon, T. Permsirivanich, N. Kanjanasoontorn, C. Akkaraphataworn, A. Seubsai, K. Faungnawakij, C. Warakulwit, M. Chareonpanich, J. Limtrakul, *Catal. Sci. Technol.* **2015**, *5*, 2347 – 2357.
[6] S. Saeidi, N. A. S. Amin, M. R. Rahimpour, *J. CO_2 Util.* **2014**, *5*, 66 – 81.
[7] W. Wang, S. Wang, X. Ma, J. Gong, *Chem. Soc. Rev.* **2011**, *40*, 3703 – 3727.
[8] M. D. Porosoff, B. Yan, J. G. Chen, *Energy Environ. Sci.* **2016**, *9*, 62 – 73.
[9] M. Albrecht, U. Rodemerck, M. Schneider, M. Bröring, D. Baabe, E. V. Kondratenko, *Appl. Catal. B* **2017**, *204*, 119 – 126.
[10] M. Al-Dossary, A. A. Ismail, J. L. G. Fierro, H. Bouzid, S. A. Al-Sayari, *Appl. Catal. B* **2015**, *165*, 651 – 660.
[11] L. M. Chew, P. Kangvansura, H. Ruland, H. J. Schulte, C. Somsen, W. Xia, G. Eggeler, A. Worayingyong, M. Muhler, *Appl. Catal. A* **2014**, *482*, 163 – 170.
[12] Y. H. Choi, Y. J. Jang, H. Park, W. Y. Kim, Y. H. Lee, S. H. Choi, J. S. Lee, *Appl. Catal. B* **2017**, *202*, 605 – 610.
[13] J. Wei, Q. Ge, R. Yao, Z. Wen, C. Fang, L. Guo, H. Xu, J. Sun, *Nat. Commun.* **2017**, *8*, 15174.
[14] M. Zhang, R. Lan, J. Liu, X. Chen, W. Zhou, *J. Chem. Soc. Faraday Trans.* **1992**, *88*, 637 – 644.
[15] J. C. Park, D. H. Chun, J.-I. Yang, H.-T. Lee, S. Hong, G. B. Rhim, S. Jang, H. Jung, *RSC Adv.* **2015**, *5*, 44211 – 44217.
[16] H. M. Torres Galvis, J. H. Bitter, C. B. Khare, M. Ruitenbeek, A. I. Dugulan, K. P. de Jong, *Science* **2012**, *335*, 835 – 838.
[17] R. Satthawong, N. Koizumi, C. Song, P. Prasassarakich, *Catal. Today* **2015**, *251*, 34 – 40.
[18] C. G. Visconti, M. Martinelli, L. Falbo, A. Infantes-Molina, L. Lietti, P. Forzatti, G. Iaquaniello, E. Palo, B. Picutti, F. Brignoli, *Appl. Catal. B* **2017**, *200*, 530 – 542.
[19] M. Amoyal, R. Vidruk-Nehemya, M. V. Landau, M. Herskowitz, *J. Catal.* **2017**, *348*, 29 – 39.
[20] B. Graf, M. Muhler, *Phys. Chem. Chem. Phys.* **2011**, *13*, 3701 – 3710.
[21] T. Riedel, H. Schulz, G. Schaub, K.-W. Jun, J.-S. Hwang, K.-W. Lee, *Top. Catal.* **2003**, *26*, 41 – 54.
[22] A. M. Hilmen, D. Schanke, K. F. Hanssen, A. Holmen, *Appl. Catal. A* **1999**, *186*, 169 – 188.
[23] K. Cheng, V. V. Ordomsky, M. Virginie, B. Legras, P. A. Chernavskii, V. O. Kazak, C. Cordier, S. Paul, Y. Wang, A. Y. Khodakov, *Appl. Catal. A* **2014**, *488*, 66 – 77.
[24] C. Yang, H. Zhao, Y. Hou, D. Ma, *J. Am. Chem. Soc.* **2012**, *134*, 15814 – 15821.
[25] H. Park, D. H. Youn, J. Y. Kim, W. Y. Kim, Y. H. Choi, Y. H. Lee, S. H. Choi, J. S. Lee, *ChemCatChem* **2015**, *7*, 3488 – 3494.
[26] M. K. Gnanamani, H. H. Hamdeh, G. Jacobs, D. Qian, F. Liu, S. D. Hopps, G. A. Thomas, W. D. Shafer, Q. Xiao, Y. Hu, B. H. Davis, *RSC Adv.* **2016**, *6*, 62356 – 62367.
[27] H. Schulz, T. Riedel, G. Schaub, *Top. Catal.* **2005**, *32*, 117 – 124.
[28] C. Wang, R. Firor, *Simulated Distillation System for ASTM D2887 Based on the Agilent 6890n GC*, **2005**, Agilent Technologies publication 5989-2726EN, https://www.agilent.com/cs/library/applications/5989-2726EN.pdf.
[29] B. Ravel, M. Newville, *J. Synchrotron Radiat.* **2005**, *12*, 537 – 541.

Manuscript received: August 3, 2017
Version of record online: ■■ ▮▮, 0000

*Y. H. Choi, E. C. Ra, E. H. Kim, K. Y. Kim, Y. J. Jang, K.-N. Kang, S. H. Choi, J.-H. Jang, J. S. Lee**

■■ – ■■

Sodium-Containing Spinel Zinc Ferrite as a Catalyst Precursor for the Selective Synthesis of Liquid Hydrocarbon Fuels

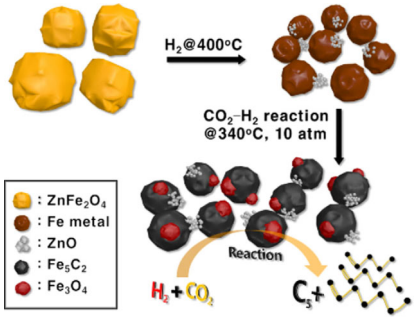

It's a gas: A catalyst derived from spinel $ZnFe_2O_4$ containing Na residue displays high CO_2 hydrogenation activity and liquid-fuel selectivity in the gasoline and diesel range with high olefin-to-paraffin ratios.